Sensors and Materials, Vol. 38, No. 9 (2026) 5215–5228
MYU Tokyo

S & M 4619

Non-wearable Image-based Method for Detecting Peak Knee Loading during Running

Cheng-Hsiu Li*

Department of Information Management, National Taitung Junior College,
No. 911, Jhengci N. Rd., Taitung, 95045 Taiwan (R.O.C.)

(Received June 9, 2026; accepted September 2, 2026)

Keywords: scientific training, key running pose, peak knee loading, non-wearable, image-based recognition

Running-related knee injuries are highly prevalent and are closely associated with excessive or poorly managed knee loading. Recent injury prevention strategies emphasize running posture and load management rather than focusing solely on local anatomical structures. In this study, a non-wearable, image-based system is proposed for detecting peak knee loading during running based on key running pose detection, providing a potential alternative to conventional hardware-based assessment methods. A geometric knee-loading region, referred to as the knee–hip–ankle (KHA) region, was defined by connecting the hip, knee, and ankle landmarks of the stance leg, and its area was computed on a frame-by-frame basis to characterize image-based knee-loading patterns. Peak knee loading was operationally defined within the Pose Method framework as the instant when the stance-leg knee joint angle reaches its minimum value, which was used in this study as a theory-driven image-based indicator for locating the key running pose. A biomechanical experiment involving six participants was conducted to examine the effects of running speed and gradient on peak knee-loading characteristics. The results showed that higher running speeds and steeper gradients were associated with enlarged KHA region areas, suggesting increased knee-loading characteristics under greater running demands. These findings demonstrate that the proposed system can capture meaningful changes in peak knee-loading characteristics and may support running posture evaluation and knee load management.

1. Introduction

Running is one of the most widely practiced aerobic exercises; however, it is also associated with a relatively high incidence of lower-extremity overuse injuries, with the knee joint being one of the most frequently affected sites. Epidemiological studies have shown that the primary clinical diagnoses of running-related knee pain are predominantly patellofemoral pain syndrome (PFPS), iliotibial band syndrome (ITBS), and patellar tendinopathy (PT).[1–3] A large-scale clinical study involving 196 runners revealed that the most common diagnoses, in descending

*Corresponding author: e-mail: chsiu.lee@gmail.com
https://doi.org/10.18494/SAM6477

ISSN 0914-4935
https://myukk.org/

order of prevalence, were PFPS, ITBS, and PT. These conditions were often accompanied by lower-limb alignment abnormalities, such as knee valgus or varus, pelvic tilt, and abnormal patellar rotation.[1] Similarly, a review focused on running-related knee pain identified PFPS, ITBS, and PT as the "three major categories" of knee injuries associated with running. These conditions commonly present as anterior or lateral knee pain, with the primary anatomical structures involved including the patellofemoral joint surface, the patellar tendon, and the iliotibial band sliding along the lateral femoral condyle.[2] These disorders are generally classified as chronic overuse injuries and are associated with the accumulation of microdamage in soft tissues under repetitive loading, muscle strength imbalances, and inadequate biomechanical control, rather than resulting from a single traumatic event.[1–3]

With respect to anterior knee pain, it has been demonstrated in both clinical practice and experimental studies that the patellofemoral joint is subjected to substantial loading during daily and training-related activities. During walking, patellofemoral joint loading is approximately 0.3–0.9 times body weight; during running, it increases to approximately 4.2–6.6 times body weight. It also increases to approximately three times body weight during stair ascent and can reach 7–8 times body weight during squatting.[4,5] More recent laboratory studies have further quantified patellofemoral joint loading across 35 weight-bearing rehabilitation exercises, revealing that greater knee flexion angles are associated with higher patellofemoral joint loading indices. In particular, movements such as single-leg decline squats can generate peak loads several times greater than those observed during walking. Consequently, these findings support the recommendation that external loads should be prescribed in a graded manner in accordance with joint load tolerance to avoid provoking or exacerbating patellofemoral pain.[4] Knee injury risk is not determined solely by the presence or absence of loading, but is closely related to the magnitude, direction, and distribution of load (including left–right symmetry), the timing of force application, and the coordination of joint and muscular load-sharing, particularly under conditions of fatigue.[4,6–12]

In recent years, perspectives on treatment and prevention have shifted from a sole focus on local anatomical structures toward an emphasis on running posture and load management. Multiple review studies have indicated that running-related knee pain has a multifactorial etiology, encompassing training errors (such as abrupt increases in running volume or intensity), insufficient lower-limb muscle strength and poor neuromuscular control, as well as abnormalities in gait and running posture.[2,3,13] Within this context, running (gait) retraining has been regarded as one of the key strategies for modifying knee joint loading. In particular, for runners with PFPS, evidence-based treatment recommendations suggest that, in addition to education and muscle strengthening, adjustments to running posture and footwear should be incorporated to facilitate the redistribution of external loads acting on the knee joint.[13]

Among gait retraining interventions, the most frequently investigated approach involves increasing the step rate through the use of a metronome or feedback cues, thereby relatively shortening step length. Multiple treatment reviews focusing on runners with patellofemoral pain (PFP) have reported that a moderate increase in step rate can reduce the knee flexion angle and knee extensor moment, decrease patellofemoral joint stress and negative knee work, and be accompanied by reductions in hip adduction angle and rearfoot eversion. Collectively, these biomechanical changes are considered beneficial for reducing mechanical loading at the knee joint.(3,13,14) Contemporary treatment perspectives centered on PFPS further emphasize that, although current evidence does not support attributing specific biomechanical abnormalities to a single causal mechanism, modifications to gait and running posture can nevertheless serve as effective strategies for symptom management and load redistribution.(13,14) In addition, research trend analyses in the PFPS literature indicate that "lower-limb kinematics and biomechanics" and "gait retraining" have emerged as major research themes in this field.(14)

Improper running posture is often associated with lower limb injuries.(15,16) Bao *et al.* investigated a recognition method for running landing actions using posture sensors, emphasizing that posture—characterized by stride frequency, gait, and landing style—is critical for injury prevention. They analyzed three landing patterns (full-foot, heel, and toe) and proposed a wearable-based monitoring system to address this issue.(15) Similarly, Li *et al.* developed a continuous detection method for abnormal running posture using wearable inertial measurement units (IMUs) in combination with deep learning models, highlighting the risks of fatigue and injury caused by improper posture despite the well-established health benefits of running.(16) In a broader perspective, van Oeveren *et al.* introduced the dual-axis framework, which categorizes running styles into five distinct types: stick, bounce, push, hop, and sit.(17)

The Pose Method is a running technique developed by Dr. Nicholas Romanov, designed to enhance running efficiency while reducing the risk of injury. Its core principle conceptualizes running as a cyclic process consisting of three main phases (Fig. 1): the key running pose, fall, and pull. The key running pose represents the moment of balance in running, when the body's center of mass is aligned over the supporting foot while the other leg lifts naturally; at this stage, the supporting knee bears the maximum load. The fall phase involves a slight forward lean of the body, utilizing gravity to shift the center of mass forward and assist propulsion. The pull phase comprises the rapid lifting of the supporting foot from the ground, minimizing ground contact time and preparing for the next step. Central to the Pose Method is the gravity-driven concept, which emphasizes using gravitational force as the primary source of propulsion rather than

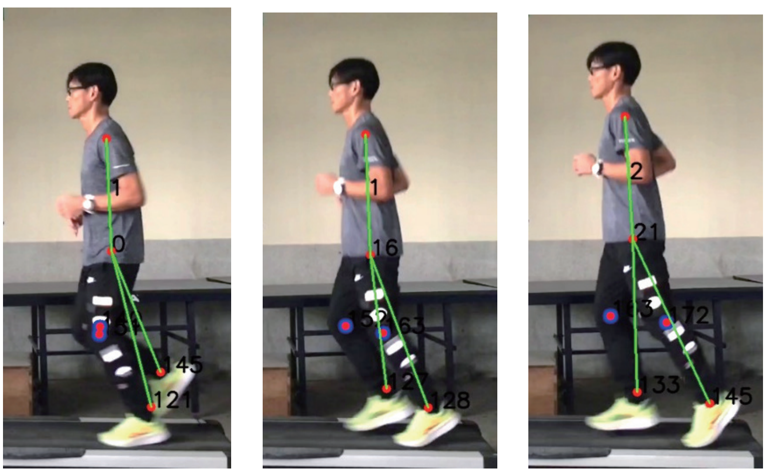

(a) (b) (c)

Fig. 1. (Color online) Analysis of running posture. (a) Key running pose, (b) fall, and (c) pull.

relying predominantly on muscular effort. By promoting a natural forward lean and minimizing unnecessary movements, this technique improves running efficiency. Furthermore, it encourages midfoot or forefoot striking to reduce impact forces and avoid excessive heel strikes, thereby lowering stress on the knees and other joints.(18)

Knee injuries are closely associated with knee loading; consequently, both clinical practice and athletic training emphasize the management of knee loading through the optimization of movement control, the strengthening of key muscle groups, and the prescription of progressive loading strategies to reduce injury risk. Accordingly, the primary aim in this study is to employ a non-hardware-based key running pose detection system grounded in image recognition techniques to investigate how peak knee loading during running can be identified through key running poses. Furthermore, the relationships between peak knee loading and a range of runner-specific factors, such as body inclination angle, running speed, and running slope, are examined in this study. The findings are intended to provide runners with practical references for running posture modification, thereby alleviating knee loading during running and reducing the risk of injury.

2. Materials

The proposed system was developed using Python, the open-source computer vision library OpenCV, and the MediaPipe Pose model. The system provides both real-time detection and video analysis functions. Running posture can be captured directly from camera images by identifying joint angles and trunk alignment, while prerecorded running videos can alternatively be imported into the system for subsequent analysis. Using the MediaPipe framework for multimedia machine learning, specifically the MediaPipe Pose model, the system applies BlazePose to estimate the midpoint of the hips, the circumscribed circle radius of the body, and the inclination angle of the line connecting the shoulders and hips. On the basis of these predictions, the system identifies the positions of 33 body pose landmarks.(19–21) In this study, the knee joint was selected as the reference point, and a knee loading triangle—referred to as the knee–hip–ankle (KHA) region—was constructed by connecting the knee (left landmark 25 and right landmark 26), the hip (left landmark 23 and right landmark 24), and the ankle (left landmark 27 and right landmark 28).

This KHA region, highlighted as the red shaded area in Fig. 2, represents the knee loading configuration during running. The following sections describe the procedures for detecting and computing the running knee-loading KHA region, as well as for identifying the KHA region corresponding to peak knee loading.

2.1 Detection and computation of the knee-loading KHA region area

First, the coordinate definition and pixel mapping are described. For any frame *t*, the joint landmarks returned by MediaPipe are represented in normalized image coordinates.

$$\boldsymbol{p}_j(t) = \left(x_j(t), y_j(t)\right), x_j, y_j \in \left[0,1\right] \tag{1}$$

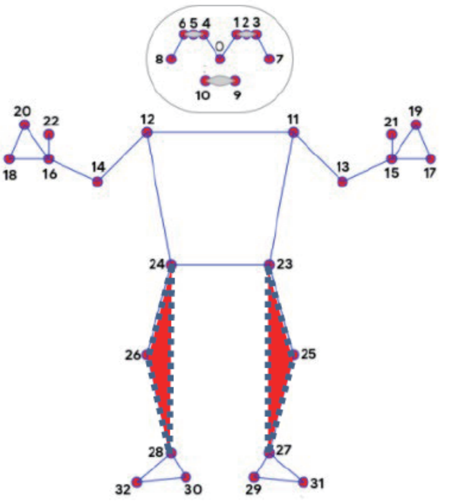

0. nose
1. left_eye_inner
2. left_eye
3. left_eye_outer
4. right_eye_inner
5. right_eye
6. right_eye_outer
7. left_ear
8. right_ear
9. mouth_left
10. mouth_right
11. left_shoulder
12. right_shoulder
13. left_elbow
14. right_elbow
15. left_wrist
16. right_wrist
17. left_pinky
18. right_pinky
19. left_index
20. right_index
21. left_thumb
22. right_thumb
23. left_hip
24. right_hip
25. left_knee
26. right_knee
27. left_ankle
28. right_ankle
29. left_heel
30. right_heel
31. left_foot_index
32. right_foot_index

Fig. 2. (Color online) Design of the KHA region for running knee loading analysis.

Equation (1) defines the normalized two-dimensional (2D) landmark coordinates of joint (j) at frame (t). Let the frame width and height be denoted as (W, H). The normalized coordinates are then mapped to pixel coordinates as follows.

$$\boldsymbol{P}_j(t) = \left(X_j(t), Y_j(t)\right) = \left(\lfloor x_j(t) \bullet W \rfloor, \lfloor y_j(t) \bullet H \rfloor\right) \tag{2}$$

Equation (2) converts the normalized landmark coordinates into pixel coordinates in the image plane. In this study, $j \in$ {hip, knee, ankle}, and the left and right limbs are denoted by L and R, respectively.

The KHA triangular region was then defined by connecting the hip, knee, and ankle landmarks of the stance leg. The left KHA triangular region is defined as Eq. (3), and the right KHA triangular region is defined as Eq. (4).

$$\Delta\left(\boldsymbol{P}_{L\_hip}(t), \boldsymbol{P}_{L\_knee}(t), \boldsymbol{P}_{L\_ankle}(t)\right) \tag{3}$$

$$\Delta\left(\boldsymbol{P}_{R\_hip}(t), \boldsymbol{P}_{R\_knee}(t), \boldsymbol{P}_{R\_ankle}(t)\right) \tag{4}$$

Equations (3) and (4) specify the left and right KHA triangular regions used for knee-loading geometry analysis, respectively. To compute the triangle area, given three points $\boldsymbol{A} = (x_1, y_1)$, $\boldsymbol{B} = (x_2, y_2)$, and $\boldsymbol{C} = (x_3, y_3)$, the area is calculated using the vector cross-product formula.

$$Area(\boldsymbol{A},\boldsymbol{B},\boldsymbol{C})=\frac{1}{2}\left|(x_2-x_1)(y_3-y_1)-(x_3-x_1)(y_2-y_1)\right| \tag{5}$$

Equation (5) gives the general 2D triangle area formula used to quantify the KHA region. Accordingly, the left and right KHA region areas at frame (t) are computed as follows.

$$A_L(t)=\frac{1}{2}\left|\det\left(\boldsymbol{P}_{L\_knee}(t)-\boldsymbol{P}_{L\_hip}(t),\boldsymbol{P}_{L\_ankle}(t)-\boldsymbol{P}_{L\_hip}(t)\right)\right| \tag{6}$$

$$A_R(t)=\frac{1}{2}\left|\det\left(\boldsymbol{P}_{R\_knee}(t)-\boldsymbol{P}_{R\_hip}(t),\boldsymbol{P}_{R\_ankle}(t)-\boldsymbol{P}_{R\_hip}(t)\right)\right| \tag{7}$$

Equations (6) and (7) apply the triangle area calculation to the left and right KHA regions, respectively. The resulting values, $A_L(t)$ and $A_R(t)$, represent the frame-by-frame image-based KHA region areas in pixel squared.

2.2 Detection of peak knee-loading KHA region

According to the Pose Method,[18] the key running pose represents the moment at which the supporting leg bears the greatest load during running. On the basis of this theoretical framework, in the present study, the timing of peak knee loading is operationally defined as the instant when the stance-leg knee joint angle reached its minimum value. This definition was used to identify the key running pose within the proposed image-based analysis system. However, because the knee loading was estimated from geometric image features rather than directly measuring internal knee joint forces, the KHA region should be interpreted as a geometric indicator of knee-loading characteristics rather than as a direct measurement of biomechanical joint load.

Taking the runner shown in Fig. 3 as an example, four stance-phase waveforms were collected from the runner's left side, as the camera was positioned on the left side relative to the running direction. When the left foot contacts the ground and the runner exhibits the key running pose, the knee bears the greatest load, and the knee joint angle reaches its minimum value (i.e., the valley point of the waveform). In this example, the detected peak knee-loading joint angles were 149, 150, and 154° (as indicated in Fig. 3). Because running posture is not fixed during locomotion, the detected joint angles vary across strides and differ among individuals.

Subsequently, in Fig. 4, the red curve represents the left knee joint angle, whereas the purple curve denotes the corresponding KHA region area. By comparing these two analytical curves, it can be observed that when the left foot makes ground contact and the knee joint reaches its minimum angle (Point A in Fig. 4), the corresponding KHA region area simultaneously reaches its maximum value (Point B in Fig. 4). This finding is consistent with the Pose Method theory, which associates the key running pose with maximal knee loading. Accordingly, the magnitude of the KHA region area can be used as an indicator to assess the loading condition experienced by the knee joint.

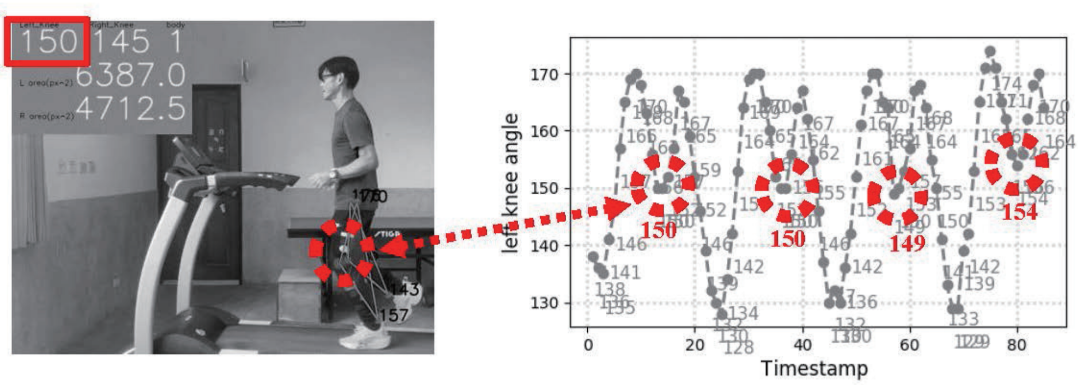

Fig. 3. (Color online) Detection of peak knee-loading KHA region.

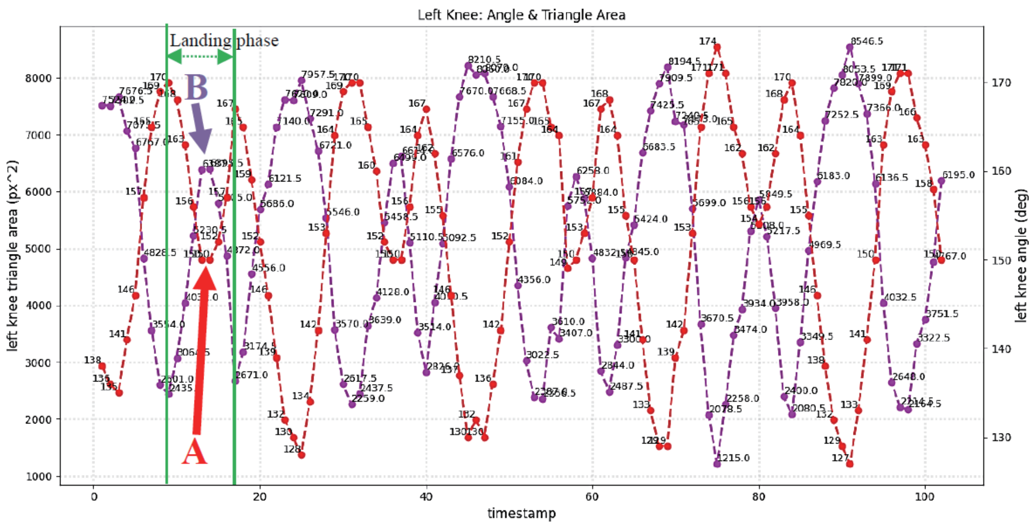

Fig. 4. (Color online) Relationship between the left knee joint angle and the KHA region area.

3. Methods

The relationships between peak knee loading and various runner-specific conditions, including body inclination angle, running speed, and running slope, were investigated through a biomechanical experimental design.

A total of six participants were recruited for the experiment. Their demographic and running-related characteristics are summarized in Table 1. Prior to participation, all participants were fully informed of the experimental procedures and provided informed consent. The participants were male runners aged 19–21 years, with a mean age of 19.67 ± 0.82 years. Their heights ranged from 172 to 181 cm, with a mean height of 176.08 ± 3.67 cm, and their body weights ranged from 67 to 89.5 kg, with a mean body weight of 79.88 ± 8.44 kg. The participants also differed in running proficiency, including experienced runners, ordinary runners, and less experienced runners. These characteristics were recorded to provide contextual information for interpreting interindividual differences in knee-loading patterns.

Table 1
Participant characteristics.

Participant	Age (years)	Sex	Height (cm)	Body weight (kg)	Running proficiency
P1	20	Male	172.0	67.0	Experienced
P2	20	Male	176.0	80.0	Ordinary
P3	21	Male	174.0	82.0	Less experienced
P4	19	Male	181.0	89.5	Experienced
P5	19	Male	180.0	87.2	Ordinary
P6	19	Male	173.5	73.6	Ordinary
Mean ± SD	19.67 ± 0.82	—	176.08 ± 3.67	79.88 ± 8.44	—

During the experiment, participants' running habits were recorded. Each participant was instructed to run under two experimental conditions: (1) running at six different speeds on the same slope, with each trial lasting 15 s, and (2) running under seven different slope conditions at the same running speed, with each trial lasting 15 s. Throughout all trials, running posture images were captured using the system developed in this study.

After the experiment, kinematic data were extracted from the recorded running videos, and statistical analyses were performed to examine the relationships between peak knee loading and the investigated factors, including body weight, height, body inclination angle, running speed, and running slope.

4. Results and Discussion

The experimental results obtained under different running speeds and gradients are discussed separately below. Representative images of the experimental setup and system-based posture detection are shown in Fig. 5. The results are presented as group-level comparisons across the six participants, focusing on changes in knee joint angle at the key running pose, KHA region area, and body inclination angle under different running conditions. Given the exploratory nature of the study and the relatively small sample size, the findings should be interpreted as preliminary evidence of the feasibility of the proposed image-based analysis method rather than as fully generalizable biomechanical conclusions.

4.1 Analysis of running speed conditions

The proposed system was used to analyze the key running pose and corresponding knee-loading indicators under six levels of running speed. The group-level descriptive results across the six participants are summarized in Table 2, and the corresponding integrated trends are illustrated in Fig. 6. The analyzed variables included the knee joint angle at the key running pose, the KHA region area, and the body inclination angle.

Across the six participants, running speed showed a clear group-level association with the measured knee-loading indicators. As shown in Table 2 and Fig. 6, when running speed increased from level 3 to level 8, the mean knee joint angle at the key running pose decreased from 162.37 to 154.03°, indicating greater knee flexion at higher speeds. In contrast, the mean KHA region area increased from 2871.8 to 4074.3 px^2, suggesting that higher running speeds

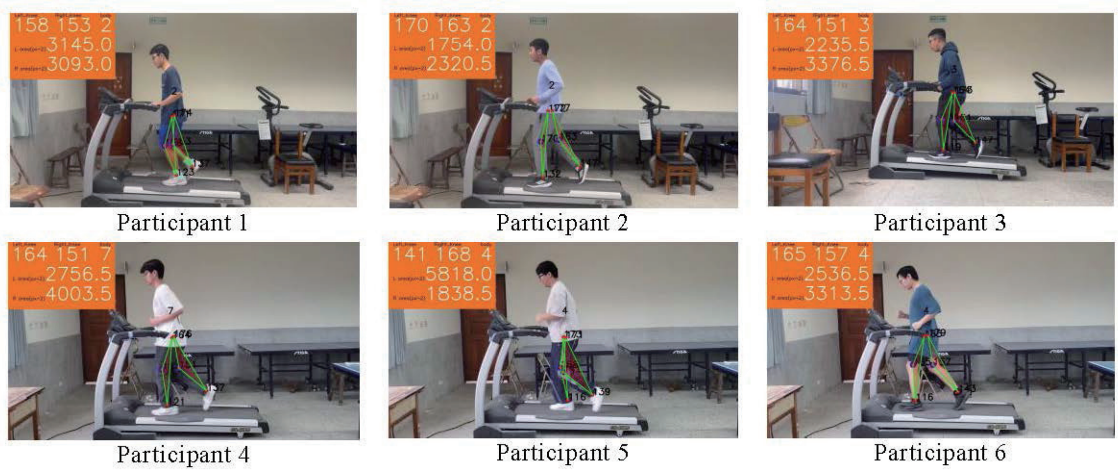

Fig. 5. (Color online) Representative images of participants during the experiment.

Table 2
Group-level results under different running speeds.

Running speed	Knee angle mean ± SD	KHA area mean ± SD	Body inclination mean ± SD
3	162.37 ± 4.63	2871.8 ± 655.3	1.96 ± 1.32
4	158.81 ± 5.64	3281.6 ± 665.6	2.54 ± 1.10
5	157.85 ± 5.38	3552.2 ± 740.9	2.93 ± 1.00
6	156.72 ± 3.96	3742.4 ± 487.0	3.55 ± 1.55
7	154.57 ± 3.41	3983.1 ± 347.6	3.87 ± 1.63
8	154.03 ± 3.40	4074.3 ± 435.7	4.42 ± 2.01

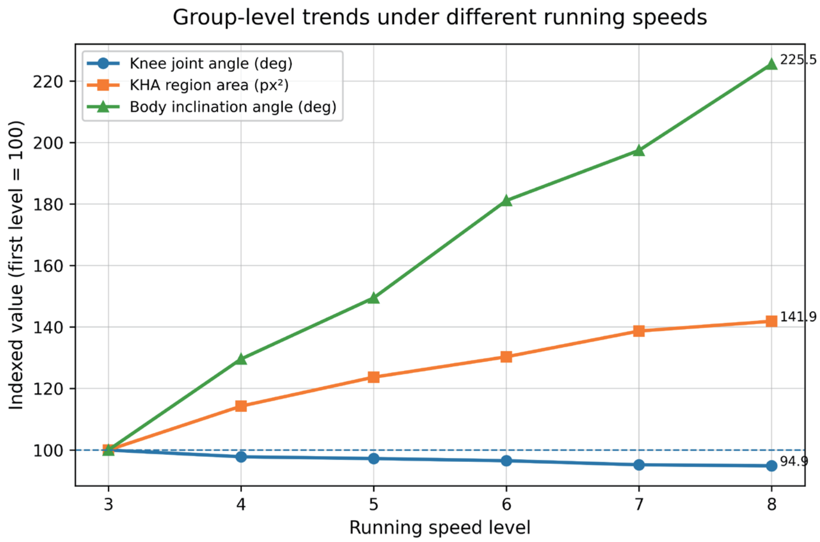

Fig. 6. (Color online) Group-level trends in knee joint angle, KHA region area, and body inclination angle under different levels of running speed. Values were normalized to the first running speed level to facilitate the integrated comparison across variables with different units.

were associated with an enlarged knee-loading geometry. The mean body inclination angle also increased from 1.96 to 4.42°, indicating a tendency toward greater forward inclination at higher running speeds.

Overall, the group-level results from the six participants demonstrated a consistent relationship between increased running speed and increased knee-loading characteristics at the key running pose. Higher running speeds were associated with smaller knee joint angles and larger KHA region areas, whereas body inclination angle showed a moderate increasing tendency as running speed increased. These observations align with recent biomechanical findings indicating that increasing running speed systematically alters knee kinetics and kinematics, including reductions in knee flexion excursion and increases in joint loading parameters. For example, prior work has shown that higher running speeds are accompanied by increased joint kinetics and altered knee mechanics consistent with heightened loading demands.(22,23) Although an interindividual variation was observed across participants, the integrated group-level comparison indicated a general trend in which higher running speeds corresponded to reduced knee joint angles, enlarged KHA region areas, and slightly increased trunk inclination. These findings indicate that running speed plays a critical role in affecting knee-loading characteristics during the key running pose, while individual differences in body characteristics and running proficiency may further modulate the magnitude of knee-loading responses.

4.2 Analysis of gradient conditions

The proposed system was further used to analyze the key running pose and corresponding knee-loading indicators under seven gradient levels at the same running speed. The group-level descriptive results across the six participants are summarized in Table 3, and the corresponding integrated trends are illustrated in Fig. 7. The analyzed variables included the knee joint angle at the key running pose, the KHA region area, and the body inclination angle.

Across the six participants, gradient level was also associated with changes in knee-loading indicators. As shown in Table 3 and Fig. 7, when the gradient increased from level 1 to level 7, the mean knee joint angle at the key running pose decreased from 158.25 to 153.38°, whereas the mean KHA region area increased from 3518.7 to 4001.7 px^2. The mean body inclination angle showed a modest increase from 3.04° at gradient level 1 to 4.11° at gradient level 6, followed by a slight decrease to 3.66° at gradient level 7. This nonlinear pattern suggests that trunk inclination may not increase proportionally with treadmill gradient. Instead, runners may adjust their posture differently under steeper conditions, possibly owing to individual running strategies, stride regulation, or short-term adaptation to increased external demands.

Overall, the group-level results from the six participants indicated that increasing running gradient was generally associated with elevated knee-loading characteristics at the key running pose, as reflected by enlarged KHA region areas. While changes in knee joint angle were less pronounced than those in KHA region area, the mean knee joint angle showed a slight decreasing tendency across gradient levels, suggesting a modest increase in knee flexion under steeper running conditions. The body inclination angle showed a generally increasing but nonlinear

Table 3
Group-level results under different gradients.

Gradient	Knee angle mean ± SD	KHA area mean ± SD	Body inclination mean ± SD
1	158.25 ± 4.20	3518.7 ± 678.4	3.04 ± 1.97
2	155.65 ± 5.36	3761.3 ± 638.6	3.62 ± 2.10
3	156.38 ± 4.77	3695.4 ± 671.3	3.69 ± 1.77
4	155.38 ± 4.92	3805.5 ± 584.8	3.76 ± 1.92
5	155.07 ± 5.49	3827.4 ± 613.9	4.07 ± 1.59
6	154.44 ± 5.24	3962.1 ± 709.0	4.11 ± 1.63
7	153.38 ± 5.75	4001.7 ± 644.6	3.66 ± 1.97

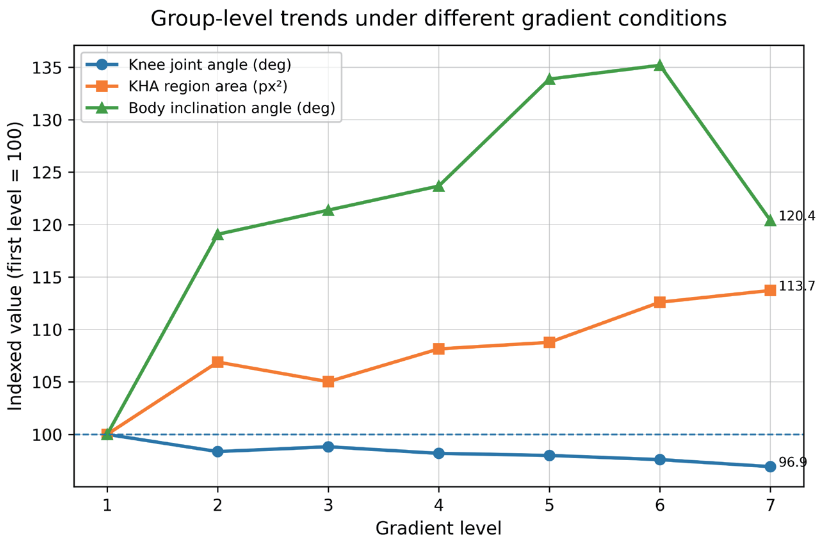

Fig. 7. (Color online) Group-level trends in knee joint angle, KHA region area, and body inclination angle under different gradient conditions. Values were normalized to the first gradient level to facilitate integrated comparison across variables with different units.

tendency across gradient levels, indicating that runners may adjust trunk posture in response to increased external demands. These observations are supported by recent biomechanical evidence showing that graded running imposes distinct mechanical demands on lower limb joints and alters joint mechanics, kinematics, and neuromuscular responses compared with level running, particularly under uphill and downhill conditions.[24] Although an interindividual variation was observed across participants, the integrated group-level comparison suggested a general trend in which steeper gradients corresponded to enlarged KHA region areas and modest changes in knee angle and trunk inclination. These findings suggest that running gradient affects knee-loading characteristics during the key running pose primarily through increased external demands and posture adjustments, while individual body characteristics and running proficiency may further affect the magnitude of the knee-loading response.

5. Conclusions

In this study, a non-wearable, image-based key running pose detection system for identifying peak knee loading during running was proposed. By integrating computer vision techniques with biomechanical concepts derived from the Pose Method, a geometric KHA region was defined and quantified to represent knee loading characteristics at the key running pose. The proposed approach enables the estimation of peak knee loading without the need for wearable sensors or force-measurement devices, thereby providing a practical and accessible alternative for running posture assessment.

Experimental results demonstrated that, under the Pose-Method-based operational definition used in this study, peak knee loading was identified at the point when the stance-leg knee joint angle reached its minimum value, corresponding to the key running pose. Moreover, the magnitude of the KHA region area exhibited a clear association with knee-loading characteristics, supporting its use as an image-based geometric indicator, rather than a direct force measurement, for assessing peak knee loading within the proposed image-based framework. However, because the KHA region area was derived from 2D landmark geometry, it should be interpreted as a proxy for knee-loading characteristics and not as a quantified measure of actual knee joint load or ground reaction force in newtons. The group-level analyses across six participants further revealed that increased running speed and steeper gradients were generally associated with enlarged KHA region areas, whereas changes in knee joint angle were relatively moderate. The body inclination angle also showed a tendency to increase under higher running speed and gradient conditions, suggesting that trunk posture adjustments may contribute to knee-loading modulation under increased external demands.

The findings of this study highlight the effects of running speed and slope on knee loading during the key running pose and underscore the importance of posture-based load management in running injury prevention. The proposed system offers runners and coaches an intuitive and non-invasive tool for identifying peak knee loading events and for evaluating how running posture and environmental conditions affect knee loading. Such information may serve as a practical reference for running posture modification and training load adjustment aimed at reducing knee injury risk.

Several limitations should be acknowledged. First, although the sample size was increased to six participants, the participant group remained relatively small and consisted only of male runners; therefore, the results should still be interpreted as preliminary and may not be generalizable to all runner populations. In future studies, larger and more diverse participant samples should be recruited, including runners of different genders, ages, and running proficiency levels. Second, knee loading was inferred from geometric features rather than directly measured joint forces. Third, the experiments were conducted under treadmill-running conditions. Although treadmill testing allowed the running speed and gradient to be controlled, treadmill running may differ from overground running in lower-limb kinetics, stride regulation, surface interaction, and propulsion mechanics. Therefore, the present findings may not be directly generalizable to outdoor running environments. Future studies should include overground running tests on different surfaces, such as asphalt, track surfaces, and grass, to evaluate the robustness and practical applicability of the proposed method. Fourth, the proposed system was based on 2D image analysis; therefore, the estimated knee joint angles and KHA region areas may be affected by 2D projection errors, perspective distortion, out-of-plane limb motion, and partial occlusion during running. The accuracy of the proposed method depends on the camera viewpoint. In particular, a sagittal-side view is required to obtain reliable lower-limb geometry, and deviations from this viewpoint may affect the calculated knee angle and KHA region area. Future studies should involve a larger cohort, statistical modeling, and the validation of the proposed indicators against force-plate measurements or musculoskeletal simulations. In addition, multiview camera settings, camera calibration procedures, depth sensing, or three-dimensional pose estimation should be considered in future work to reduce viewpoint dependence and improve measurement robustness. Despite these limitations, the results of the present study demonstrate the feasibility and potential value of using key running pose detection and KHA region analysis as a non-wearable approach for assessing peak knee loading during running.

Acknowledgments

This study was supported by the National Science and Technology Council of Taiwan (grant number NSTC 114-2637-E-602-002-).

References

1 E. Benca, S. Listabarth, F. K. J. Flock, E. Pablik, C. Fischer, S. M. Walzer, R. Dorotka, R. Windhager, and P. Ziai: J. Clin. Med. **9** (2020) 438. https://doi.org/10.3390/jcm9020438
2 N. Gizińska, A. Górniak, A. Rusiecka, A. Kubas, P. Lewandowska, A. Sobczyk, and M. Widawski: Qual. Sport **42** (2025) 60455. https://doi.org/10.12775/QS.2025.42.60455
3 S. Mellinger and G. A. Neurohr: Ann. Transl. Med. **7** (2019) S249. https://doi.org/10.21037/atm.2019.04.08
4 K. Song, S. R. Scattone, T. J. Hullfish, K. G. Silbernagel, and J. R. Baxter: Am. J. Sports Med. **51** (2023) 2110. https://doi.org/10.1177/03635465231175160
5 B. H. Alsulaimani: MOJ Orthop. Rheumatol. **11** (2019) 31. https://doi.org/10.15406/mojor.2019.11.00465
6 Z. Gao, L. Xiang, H. Jiang, Q. Mei, G. Fekete, J. S. Baker, and Y. Gu: BMC Sports Sci. Med. Rehabil. **17** (2025) 337. https://doi.org/10.1186/s13102-025-01372-3
7 M. Belkhelladi, T. Cierson, and P. A. Martineau: Orthop. J. Sports Med. **13** (2025) 23259671241312681. https://doi.org/10.1177/23259671241312681
8 X. Li and L. Mao: Sensors **25** (2025) 6301. https://doi.org/10.3390/s25206301
9 C. Liu, W. Peng, W. Qu, Z. Zhang, J. Sun, J. He, B. Cheng, and D. Li: PLoS One **20** (2025) e0321925. https://doi.org/10.1371/journal.pone.0321925
10 W. Wang, S. Xu, I. Komnik, J. Viellehner, M. Zedler, and W. Potthast: Sports Med. Open **11** (2025) 22. https://doi.org/10.1186/s40798-025-00824-x
11 A. Encarnación-Martínez, E. Sánchez-Ribes, R. Bruna-Lázaro, R. Sanchis-Sanchis, J. Ashby, and P. Pérez-Soriano: Sports Med. Open **11** (2025) 107. https://doi.org/10.1186/s40798-025-00878-x
12 N. Kakouris, N. Yener, and D. T. P. Fong: J. Sport Health Sci. **10** (2021) 513. https://doi.org/10.1016/j.jshs.2021.04.001
13 A. Santanello, M. Volokitin, P. Matthew, A. Modica, C. McKellar, K. Thakkar, M. Schear, A. Tai, J. Nagler, and S. Suarez: J. Osteopath. Med. **125** (2025) 135. https://doi.org/10.1515/jom-2024-0006
14 J. Xu, Z. Cai, M. Chen, X. Wang, X. Luo, and Y. Wang: Front. Med. **11** (2024) 1370258. https://doi.org/10.3389/fmed.2024.1370258
15 Z. Bao, X. Zhao, X. Zhang, R. Pan, S. Pang, and H. Wang: Proc. 2023 IEEE Int. Conf. Smart Internet of Things (IEEE, 2023) 154–161. https://doi.org/10.1109/SmartIoT58732.2023.00029

16 X. Li, H. Wang, Y. Li, H. Zhang, and F. Sun: Proc. 2024 Int. Conf. Sports Technology and Performance Analysis (ACM, 2024) 52–59. https://doi.org/10.1145/3723936.3723945

17 B. T. van Oeveren, C. J. de Ruiter, P. J. Beek, and J. H. van Dieën: Sports Biomech. **23** (2021) 516. https://doi.org/10.1080/14763141.2021.1873411

18 Pose Method: https://posemethod.com/running/ (accessed December 18, 2024).

19 V. Bazarevsky and I. Grishchenko: On-Device Real-Time Body Pose Tracking with MediaPipe BlazePose (Google Research). https://ai.googleblog.com/2020/08/on-device-real-time-body-pose-tracking.html (accessed December 18, 2024).

20 Google Developers: MediaPipe Pose. https://developers.google.com/mediapipe/solutions/vision/pose_landmarker/ (accessed December 18, 2024).

21 C. H. Li: Int. J. Eng. Technol. Innovation **15** (2025) 99. https://doi.org/10.46604/ijeti.2024.13851

22 K. A. Knurr, D. G. Cobian, S. A. Kliethermes, M. R. Joachim, and B. C. Heiderscheit: Med. Sci. Sports Exerc. **56** (2024) 1233. https://doi.org/10.1249/MSS.0000000000003409

23 B. Van Hooren, I. Jukic, M. Cox, K. G. Frenken, I. Bautista, and I. S. Moore: Sports Med. **54** (2024) 1269. https://doi.org/10.1007/s40279-024-01997-3

24 Z. Lu, B. Suo, L. Deng, J. Wang, W. Fu, Y. Zhong, and J. Jin: Front. Bioeng. Biotechnol. **13** (2025) 1690023. https://doi.org/10.3389/fbioe.2025.1690023